Structure of the Dithionite-Generated Tryptophan Tryptophylquinone Cofactor Radical in Methylamine Dehydrogenase Revealed by ENDOR and ESEEM Spectroscopies

Kurt Warncke,[1a,†] Harold B. Brooks,[1b] Hong-in Lee,[1a] John McCracken,[1a] Victor L. Davidson,[1b] and Gerald T. Babcock*,[1a]

Contribution from the Department of Chemistry, Michigan State University, East Lansing, Michigan 48824, and Department of Biochemistry, The University of Mississippi Medical Center, Jackson, Mississippi 39216

Received January 30, 1995[⊗]

Abstract: The structure of the tryptophan tryptophyl-semiquinone cofactor in frozen solutions of randomly-oriented methylamine dehydrogenase from *Paracoccus denitrificans* has been characterized by continuous wave-electron nuclear double resonance (CW-ENDOR) and electron spin echo envelope modulation (ESEEM) spectroscopic analyses of hyperfine and nuclear quadrupole interactions. The radical was generated by direct reduction of the oxidized enzyme with dithionite in ^1H_2O or ^2H_2O buffer. Multifrequency ESEEM studies reveal weak hyperfine interactions with two nitrogen nuclei that have ^{14}N nuclear quadrupole coupling parameters consistent with indole nitrogen present in the two tryptophan side chains that are cross-linked covalently to form the cofactor. Analysis of nonsolvent exchangeable hyperfine couplings in ^1H ENDOR powder spectra yields the rhombic hyperfine tensors for two α-^1H and three β-^1H interactions, which are assigned to the two $C-H_\alpha$ interactions on the *ortho*-quinone-modified indole ring and the two pairs of β-methylene-^1H of the indole and indole-quinone rings. The pairs of methylene $C_\beta-^1H$ bonds are oriented relative to the ring plane normals at dihedral angles, θ, of (55°, 65°) and (~60°, ~60°). Analysis of orientation-restricted ENDOR spectra shows that the indole ring planes are rotated by the dihedral angle, χ, of 48° ± 11° along their covalent link. Weak matrix ^2H ESEEM suggests that the unpaired spin density (ϱ_π) is localized predominantly on the buried indole-quinone ring, away from the unmodified indole that extends to the protein solvent accessible surface. Absence of strong exchangeable α-hydrogen hyperfine couplings in ^1H ENDOR and ^2H ESEEM spectra suggests that the quinonoid oxygen atoms are deprotonated and, therefore, that the radical is negatively charged. The θ and χ values in the TTQ semiquinone are the same within error as those determined previously for oxidized TTQ by X-ray crystallographic analyses. Thus, redox state changes do not trigger significant conformational changes in the cofactor or surrounding protein medium in isolated methylamine dehydrogenase. Although 87% of the detected ϱ_π is localized on the indole-quinone ring, significant ϱ_π is distributed to the fused pyrrole ring of the unmodified indole, despite the suboptimal inter-ring $\pi-\pi$ conjugation geometry. Therefore, in the native cofactor oxidation reactions, chemical transformations at the active center can influence directly the inter-ring partitioning of ϱ_π.

Introduction

Methylamine dehydrogenase (MADH) from gram negative bacteria catalyzes the oxidative deamination of methylamine to generate formaldehyde, ammonia, and two reducing equivalents.[2] MADH is among an emerging class of enzymes that employ posttranslationally modified amino acid side chains as redox catalytic centers.[3,4] The amino acid-derived cofactor structure common to MADH from different bacterial species has been identified by chemical methods[4c,5] and confirmed by X-ray crystallographic analyses[6] as two tryptophan indole side chains that are cross-linked covalently. One of the six-membered rings is modified further with an *ortho*-carbonyl function. The structure of the oxidized tryptophan tryptophylquinone cofactor (TTQ) is depicted in Figure 1.

The TTQ cofactor performs a dual role as a center for bond-making and bond-breaking chemistry and as an electron-transfer cofactor. Addition of methylamine substrate to MADH promotes rapid formation of a two-electron reduced hydroquinone form of TTQ with concommitant covalent incorporation of the amine nitrogen atom and release of product formaldehyde.[9−13] Amine nitrogen substitution appears to occur at $C_{6'}$.[8] In the subsequent oxidative half-reaction *in vivo*, two reducing equiva-

† Present address: Department of Physics, Emory University, Atlanta, GA 30322.

⊗ Abstract published in *Advance ACS Abstracts*, September 15, 1995.

(1) (a) Michigan State University. (b) University of Mississippi Medical Center.

(2) Davidson, V. L. *Principles and Applications of Quinoproteins*; Davidson, V. L., Ed.; Marcel Dekker, Inc.: New York, 1993.

(3) Dooley, D. M.; McGuirl, M. A.; Brown, D. E.; Turowski, P. N.; McIntire, W. S.; Knowles, P. F. *Nature* **1991**, *349*, 262−264.

(4) (a) Janes, S. M.; Mu, D.; Wemmer, D.; Smith, A. J.; Kaur, S.; Maltby, D.; Burlingame, A. L.; Klinman, J. P. *Science* **1990**, *248*, 981−987. (b) Ito, N.; Phillips, S. E. V.; Steven, C.; Ogel, Z. B.; McPherson, M. J.; Keen, J. N.; Yadav, K. D. S.; Knowles, P. F. *Nature* **1991**, *350*, 87−90. (c) McIntire, W. S.; Wemmer, D. E.; Chistoserdov, A.; Lidstrom, M. E. *Science* **1991**, *252*, 817−824. (d) Babcock, G. T.; Barry, B. A.; Debus, R. J.; Hoganson, C. W.; Atamian, M.; McIntosh, L.; Sithole, I.; Yocum, C. F. *Biochemistry* **1989**, *28*, 9557−9565. (e) Klinman, J. P.; Mu, D. *Ann. Rev. Biochem.* **1994**, *63*, 299−344. (f) Sigel, H.; Sigel, A. *Metal Ions in Biological Systems, Volume 30: Metalloenzymes Involving Amino Acid Residue and Related Radicals*; Marcell Dekker: New York, 1994.

(5) Chistoserdov, A. Y; Tsygankov, Y. D.; Lidstrom, M. E. *Biochem. Biophys. Res. Comm.* Davidson, V. L. *Methods Enzymol.* **1990**, *188*, 241−246.

(6) Chen, L.; Mathews, F. S.; Davidson, V. L.; Huizinga, E. G.; Vellieux, F. M. D.; Duine, J. A.; Hol, W. G. *F.E.B.S. Lett* **1991**, *287*, 163−166.

(7) Chen, L.; Mathews, F. S.; Davidson, V. L.; Huizinga, E. G.; Vellieux, F. M. D.; Hol, W. G. J. *Proteins* **1992a**, *14*, 288−299.

0002-7863/95/1517-10063$09.00/0

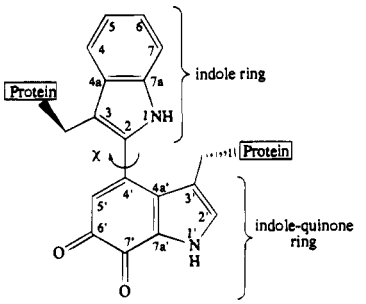

Figure 1. Structure of the oxidized tryptophan tryptophylquinone (TTQ) cofactor in methylamine dehydrogenase from *Paracoccus denitrificans*.[6,7] A comparable TTQ structure was obtained for MADH from *Thiobacillus versutus*.[8] In this work, the unmodified and 6′,7′-*ortho*-carbonyl-modified side chains are referred to as the indole and indole-quinone rings, respectively. The cofactor is formed from the covalently cross-linked side chains of the gene-encoded tryptophan residues 57 (indole-quinone ring) and 107 (indole ring) of the large subunit. The ring−ring dihedral angle, χ, is 42°, corresponding to a rotation of the fused pyrrole ring of the indole-quinone system out of the plane of the page by χ. The orientation of the β-methylene link to the polypeptide backbone, with respect to the ring faces, is shown.

lents are transferred to the blue copper protein, amicyanin.[14] Observation of a metastable aminosemiquinone intermediate during controlled *in vitro* oxidation of substrate-reduced MADH,[15] and the one-electron capacity of the copper center, suggests that the two electrons are transferred sequentially. In the native reaction, transfer of the second electron from cofactor to amicyanin is required for release of the substrate nitrogen as ammonia and regeneration of the resting, fully-oxidized state of the enzyme.[13] A sequential pathway through an iminosemiquinone intermediate has also been established for the amine oxidation reaction mediated by the tyrosine-derived topa-quinone cofactor of amine oxidases.[3,16]

A principal focus of investigations of the molecular mechanism of oxidation of the TTQ hydroquinone and semiquinone species is the degree of coupling between the bond-making, bond-breaking (adiabatic) active site chemistry and the long-range (nonadiabatic) electron transfer reactions that promote amicyanin reduction.[2,13,17,18] Coupling of these reactions is intimated by the X-ray crystallographic structures of MADH.[6−8] The active site on the indole-quinone ring is located within the protein interior, while the indole ring extends toward and then breachs with C_5 and C_6, the solvent accessible surface of the protein.[6,7] Thus, reducing equivalents generated at the active center can, in principle, traverse intramolecularly to protein-external oxidants. Indeed, in cocrystals of MADH and amicyanin,[19] atoms C_5 and C_6 are located at the contact surface of the MADH−amicyanin complex and achieve the shortest TTQ edge-to-copper distance of 9 Å. Parallel stopped-flow kinetic studies of MADH oxidation by amicyanin have been performed by using the practicably generated and manipulated dithionite-reduced TTQ hydroquinone and stable semiquinone species.[17,18] Analysis of the temperature-dependence of the oxidation rates by using Marcus theory revealed a relatively strong donor−acceptor electronic coupling matrix element, H_{AB}.[17,18] In the MADH−amicyanin cocrystal,[19] this H_{AB} value would be consistent with electron departure from the C_4-C_7 edge of the indole ring, according to both direct[20] and path-selective[21] treatments of electron transmission.[17] However, the dihedral angles, χ, of 42° and 40° between the indole and indole-quinone rings in oxidized TTQ in *Paracoccus denitrificans* and *Thiobacillus versutus* MADH[6−8] suggest suboptimal inter-ring $\pi-\pi$ conjugation.[10,17] A reorientation of the cofactor rings toward a conformation that would enhance delocalization of the transferrable electron to the unmodified indole ring has been suggested on the basis of the significant activation energy barrier (reorganization energy, 2.3 eV) associated with oxidation of the dithionite-generated hydroquinone and semiquinone species.[17,18]

In the present work, we address redox-linked changes in the nuclear geometry and electronic structure of the TTQ cofactor from MADH of *P. denitrificans* that may influence reactivity by characterizing the semiquinone state of TTQ prepared by single electron reduction of oxidized enzyme with dithionite.[22] Comparison of the dithionite-reduced semiquinone structure with the atomic structures for the oxidized state of the enzyme determined by X-ray crystallography[6−8,19] allows an assessment of the influence of redox-linked changes in protein-cofactor solvation and electronic resonance energies on the TTQ-protein structure. Unlike the native aminosemiquinone formed following oxidation of substrate-reduced TTQ, dithionite reduction forms the TTQ radical directly from the oxidized state.[22] Thus, comparisons with the structure of the aminosemiquinone species derived from substrate-reduced MADH[13,23] will reveal changes introduced specifically by covalent incorporation of the amine substrate.[24] The detailed electronic structure information required for this analysis is obtained by using the electron spin echo envelope modulation (ESEEM) technique of pulsed-electron paramagnetic resonance spectroscopy[25] (EPR) and continuous-wave electron nuclear double resonance[26] (CW-ENDOR). Analysis of the ^{14}N, ^{1}H, and ^{2}H electron-nuclear hyperfine and ^{14}N nuclear quadrupole interactions in the dithionite-generated TTQ semiquinone maps partially the unpaired spin density distribution in the radical and reveals the

(8) Huizinga, E. G.; van Zanten, B. A. M.; Duine, J. A.; Jongejan, J. A.; Hultema, F.; Wilson, K. S.; Hol, W. G. J. *Biochemistry* **1992**, *31*, 9789−9795.
(9) Kenney, W. C.; McIntire, W. *Biochemistry* **1983**, *22*, 3858−3868.
(10) Backes, G.; Davidson, V. L.; Huitema, F.; Duine, J. A.; Sanders-Loehr, J. *Biochemistry* **1991**, *30*, 9201−9210.
(11) Davidson, V. L.; Jones, L. H.; Graichen, M. E. *Biochemistry* **1992**, *31*, 3385−3390.
(12) Brooks, H. B.; Jones, L. H.; Davidson, V. L. *Biochemistry* **1993**, *32*, 2725−2729.
(13) Warncke, K.; Brooks, H. B.; Babcock, G. T.; Davidson, V. L.; McCracken, J. *J. Am. Chem. Soc.* **1993**, *115*, 6464−6465.
(14) Husain, M.; Davidson, V. L. *J. Biol. Chem.* **1985**, *260*, 14626−14629.
(15) Davidson, V. L. *Methods Enzymol.* **1990**, *188*, 241−246.
(16) (a) McCracken, J.; Peisach, J.; Cote, C. E.; McGuirl, M. A.; Dooley, D. M. *J. Am. Chem. Soc.* **1992**, *114*, 3715−3720. (b) Turowski, P. N.; McGuirl, M. A.; Dooley, D. M. *J. Biol. Chem.* **1993**, *268*, 17660−17682. (c) Warncke, K.; Babcock, G. T.; Dooley, D. M.; McGuirl, M. A.; McCracken, J. *J. Am. Chem. Soc.* **1994**, *116*, 4028−4037.
(17) Brooks, H. B.; Davidson, V. L. *Biochemistry* **1994**, *33*, 5696−5701.
(18) Brooks, H. B.; Davidson, V. L. *J. Am. Chem. Soc.* **1994**, *116*, 11201−11202.
(19) Chen, L.; Durley, R.; Poliks, B. J.; Hamada, K.; Chen, Z.; Mathews, F. S.; Davidson, V. L.; Satow, Y.; Huizinga, E. G.; Vellieux, F. M. D.; Hol, W. G. J. *Biochemistry* **1992a**, *31*, 4959−4964.
(20) Moser, C. C.; Keske, J. M.; Warncke, K.; Farid, R. S.; Dutton, P. L. *Nature* **1992**, *355*, 796−802.
(21) Beratan, D. N.; Betts, J. N.; Onuchic, J. N. *Science* **1991**, *252*, 1285−1288.
(22) Husain, M.; Davidson, V. L.; Gray, K. A.; Knaff, D. B. *Biochemistry* **1987**, *26*, 4139−4143.
(23) For a preliminary account, see: Warncke, K.; Brooks, H. B.; Lee, H.-I.; Babcock, G. T.; Davidson, V. L.; McCracken, J. *Biophys. J.* **1994**, *66*, A345.
(24) Warncke, K.; Brooks, H. B.; Babcock, G. T.; Davidson, V. L.; McCracken, J. **1995** (to be submitted to *J. Am. Chem. Soc.*).
(25) (a) Kevan, L.; Bowman, M. K. *Modern Pulsed and Continuous Wave Electron Spin Resonance*; John Wiley & Sons: New York, 1990. (b) Schweiger, A. *Angew. Chem., Int. Ed. Engl.* **1991**, *30*, 265−292. (c) Dikanov, S. A.; Tsvetkov, Yu. D. *Electron Spin Echo Envelope Modulation Spectroscopy*; CRC Press; Boca Raton, FL, 1993.
(26) (a) Kevan, L.; Kispert, L. D. *Electron Spin Double Resonance Spectroscopy*, Wiley & Sons: New York, 1976. (b) Lubitz, W.; Babcock, G. T. *Trends Biochem. Sci.* **1987**, *12*, 96−100. (c) Bender, C. J.; Aisen, P. *Method. Enzymol.* **1993**, 227, part D, 190−231.

conformation of both indole methylene links to the polypeptide backbone and the relative orientation of the two indole ring planes.

Materials and Methods

Protein Purification and Preparation. The purification of MADH from *Paracoccus denitrificans*[14,15] and the selective *in vitro* preparation and characterization of the dithionite-reduced state of the TTQ cofactor have been reported.[15,22] For sample preparation in ^2H_2O, MADH was dithionite reduced in ^2H_2O, and the total exposure time to the deuterated solvent was 72 h. The absolute spin concentrations of the samples in ^1H_2O and ^2H_2O buffer were determined to be 0.5 and 0.3 mM, respectively. This corresponded to 0.75 and 0.70 radicals per active site for enzyme in ^1H_2O and ^2H_2O, respectively. ^2H_2O was purchased from Sigma Chemical Company.

Continuous-Wave EPR Spectroscopy. CW-EPR spectra were obtained at X-band on a Bruker ER200D EPR spectrometer by using a Bruker TE102 EPR cavity. The external magnetic field strength was measured with a Bruker ER035M NMR gaussmeter, and the microwave frequency was measured with an EIP Microwave Model 25B frequency counter.

Continuous-Wave ENDOR Spectroscopy. ENDOR measurements were performed by using the Bruker ER2OOD EPR spectrometer with the Bruker ER250 ENDOR/TRIPLE accessory and the Bruker ER250ENB ENDOR cavity. Radiofrequency power from a Wavetek 3000-446 signal generator was directed to an ENI 3100L amplifier and subsequently into a home-built coil assembly[27] that was terminated at 50 Ω. The cavity circuit remained matched at 50 ± 10 Ω in the radiofrequency range of 10−20 MHz.

Computation of the distance- and B_0 orientation-dependence of the α-, β-, and hydrogen-bonded proton hyperfine couplings, and the mutual orientations of the β-hyperfine tensor principal axes and indole rings, was performed by using Matlab programs on Macintosh II computers.

ESEEM Spectroscopy. The home-built pulsed-EPR spectrometer used in this work has been described.[28] In the two-pulse (90°−τ−180°, where the angles describe the angular rotation of magnetization in response to the microwave pulse) and three-pulse (90°−τ−90°−T−90°) experiments, the echo amplitude is modulated as a function of the inter-pulse times τ and T, respectively, with a periodicity that corresponds to the reciprocal of the hyperfine frequencies. The hyperfine frequencies are shown directly in the spectrum obtained by Fourier transformation of the echo envelope. Reconstruction of envelope modulation that was lost in the dead time (120 ns) in two-pulse experiments, or during the time interval $\tau + T_0$, where T_0 is the initial value of the waiting time, T, in the three-pulse experiments, was performed prior to Fourier transformation as described.[29]

Computer simulation of the ESEEM data was based on the density matrix treatment of Mims.[30,31] Simulations were run on Apple Macintosh II computers or on a DEC Vaxstation 4000. The experimental dead time was included in the time domain simulations, with the dead time reconstruction[29] performed prior to Fourier transformation as in the analysis of the experimental data. The success of the ESEEM simulations was judged according to the match with the experimental three-pulse ESEEM spectra on the basis of the following constraints: (a) the magnetic field dependence of the line shape, (b) the τ suppression behavior, and (c) the envelope modulation depth.

Chart 1. Relation of Hyperfine, β-Interaction and Inter-Ring Principal Axis Systems (PAS) to the Molecular Structure of the TTQ Cofactor

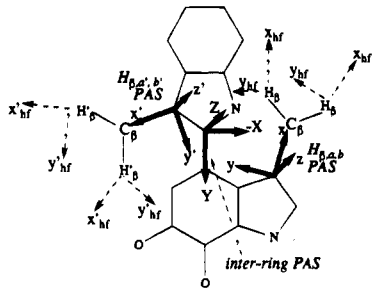

Calculation of the Mutual Orientations of the β-Methylene Groups. A. Orientation of the external magnetic field relative to the ring-β-hydrogen group. The hyperfine couplings for two β-methylene hydrogen interactions, $H_{\beta,i}$ and $H_{\beta,j}$, measured at a single radical orientation relative to the external magnetic field vector, $\mathbf{B_0}$, by ENDOR spectroscopy, can be used to estimate the orientation of B_0 relative to the molecular frame. The complete coupling tensors are obtained from analysis of powder ENDOR spectra. In the strong field approximation appropriate for these studies, the orientation of $\mathbf{B_0}$, and hence of the fictitious electron spin, S_z, with respect to the principal axes of the two hyperfine tensors is described by the polar and azimuthal angles, Θ and Φ, respectively.[32,33] For a hyperfine interaction between electron spin, $S = 1/2$, and nuclear spin, $I = 1/2$, characterized by rhombic dipolar field symmetry, the angle-dependence of the eigenfrequencies is expressed in terms of the principal components of the hyperfine tensor ($\mathbf{A}_i$) and the free nuclear Zeeman frequency (ν_N), as follows:[32,34]

$$\nu_\alpha = [(A_x/2 - \nu_N)^2 \sin^2\Theta\cos^2\Phi + (A_y/2 - \nu_N)^2 \sin^2\Theta\sin^2\Phi + (A_z/2 - \nu_N)^2\cos^2\Theta]^{1/2} \quad (1a)$$

$$\nu_\beta = [(-A_x/2 - \nu_N)^2 \sin^2\Theta\cos^2\Phi + (-A_y/2 - \nu_N)^2 \sin^2\Theta\sin^2\Phi + (-A_z/2 - \nu_N)^2\cos^2\Theta]^{1/2} \quad (1b)$$

The x, y, and z cartesian coordinates of S_z in the principal axis sytem (PAS) of the hyperfine interaction are given by sin Θ cos Φ, sin Θ sin Φ, and cos Θ, respectively.

In order to determine the unique S_z orientation that is common to the interaction of each nucleus, $H_{\beta,i}$ and $H_{\beta,j}$, in the methylene group, a molecular geometry must be assumed. Chart 1 shows the relationship of the hyperfine and reference molecular PAS that we have adopted. The two β-methylene H interactions that correspond to $H_{\beta,i}$ and $H_{\beta,j}$, are denoted $H_{\beta,a}$, $H_{\beta,b}$, and $H_{\beta,a'}$, $H_{\beta,b'}$. The mutual orientations of the hyperfine PAS and the reference molecular PAS for the β-H interactions are defined according to the assumption of sp^3-hybridized C_β and standard bond angles and bond lengths for indole.[35] For each β-H interaction, S_z in the β-interaction PAS, denoted as S_z', is related

(27) (a) Hurst, G; Kraft, K.; Schultz, R.; Kreilick, R. *J. Magn. Reson.* **1982**, *49*, 159−160. (b) Bender, C. J.; Sahlin, M.; Babcock, G. T.; Barry, B. A.; Chandrashekar, T. K.; Salowe, S. P.; Stubbe, J.; Lindstrom, B.; Petersson, L.; Ehrenberg, A.; Sjoberg, B.-M. *J. Am. Chem. Soc.* **1989**, *111*, 8076−8083. (c) Bender, C. J.; Babcock, G. T. *Rev. Sci. Instrum.* **1992**, *63*, 3523−3524.

(28) McCracken, J. L.; Shin, D.-H.; Dye, J. L. *Appl. Magn. Reson.* **1992**, *3*, 305−316.

(29) Mims, W. B. *J. Magn. Reson.* **1984**, *59*, 291−306.

(30) Mims, W. B. *Phys. Rev. B* **1972a**, *5*, 2409−2419.

(31) Mims, W. B. *Phys. Rev. B* **1972b**, *6*, 3543−3545.

(32) Hutchison, C. A.; McKay, D. B. *J. Chem. Phys.* **1977**, *66*, 3311.

(33) Wertz, J. E.; Bolton, J. R. *Electron Spin Resonance*; Chapman & Hall: New York, 1986.

(34) Dalton, L.; Kwiram, A. L. *J. Chem. Phys.* **1972**, *57*, 1132.

(35) Remers, W. A. In *Indoles, Part 1*; Houlihan, W. J., Ed.; Wiley-Interscience: New York, 1970.

to the hyperfine PAS through the 3 × 3 coordinate rotation matrices, $\mathcal{R}_i^{\dagger}$,[36] where $\mathcal{R}_i^{\dagger}$ is the adjoint of $\mathcal{R}_i$ and $i = \alpha, \beta, \gamma$ are the Euler angles, as follows:

$$S_z' = \mathcal{R}_\gamma^{\dagger}\mathcal{R}_\beta^{\dagger}\mathcal{R}_\alpha^{\dagger}S_z \qquad (2)$$

The value of γ is zero for the molecular symmetries considered here. The particular values of α and β are dependent upon the dihedral angle, θ, between the C−H$_\beta$ bond and ring p-orbital vectors about the C$_\beta$−C$_{ring}$ bond. As detailed in the Discussion, the value of θ can be extracted from the isotropic hyperfine couplings of the two β-H-methylene nuclei that are derived from the complete hyperfine tensors. Since there is only one value of S_z' for both H$_{\beta,a}$ and H$_{\beta,b}$ hyperfine interactions at a single molecular orientation, the two vector eqs 2 for each β-H interaction can be solved to reveal the coordinates of the common S_z' vector.

B. Mutual Orientation of Two β-Methylene Interactions. The mutual orientation of the PAS of two different β-H methylene interactions can be computed from coordinate transformations in the manner described in part A. For the particular case of the TTQ cofactor, there are two spatially separated β-methylene interactions that are located on the indole and indole-quinone rings. We assume that the mutual orientation of the ring planes is determined only by the dihedral angle, χ, about the C$_2$−C$_{4'}$ bond, as depicted in Figure 1. For a single molecular orientation, the hyperfine couplings for the β-H nuclei in the methylene group of the indole ring can be calculated from the orientation of S_z', defined by the indole-quinone β-H nuclei, as a function of χ. This method of calculating χ, from the match of the calculated and observed indole ring β-H methylene hyperfine coupling, is advantageous because it allows easy assessment of the uniqueness and uncertainty of the solution. The direction of the fictitious spin in the β-H methylene reference PAS of the indole ring, S_z'', is given by

$$S_z'' = \mathcal{R}'_\beta{}^{\dagger}\mathcal{R}'_\alpha{}^{\dagger}\mathcal{R}_\beta{}^{\dagger}\mathcal{R}_\alpha{}^{\dagger}S_z' \qquad (3)$$

Here, the $\mathcal{R}$ and $\mathcal{R}'$ represent rotations into and out of a reference coordinate system relating the two rings, shown as the inter-ring PAS in Chart 1. By using this method, the angle β in $\mathcal{R}'$ is equal to χ. Equation 2, followed by eqs 1a and 1b, are used to relate S_z'' to the hyperfine PAS for each indole ring β-H nucleus and thus to calculate the corresponding hyperfine coupling.

Results

CW-EPR Spectroscopy. Figure 2 shows CW-EPR spectra of dithionite-reduced MADH oriented randomly in frozen ^1H_2O and ^2H_2O buffer. The inhomogeneously broadened line shape displays a modest anisotropy of the **g**-tensor. The line shape of the radical in ^1H_2O buffer is comparable with that observed previously in Q-band (33.5 GHz) EPR studies of MADH in a lyophilized powder sample.[37] Solvent exchange in ^2H_2O diminishes the peak-to-trough width of the EPR line shape by 0.1 mT. This small effect shows that interaction of the unpaired spin density with solvent-exchangeable protons is relatively weak. Characterization of the unresolved electron-nuclear hyperfine interactions that contribute to the EPR line broadening requires the deployment of high-resolution techniques of EPR spectroscopy that address directly the radiofrequency hyperfine transitions.

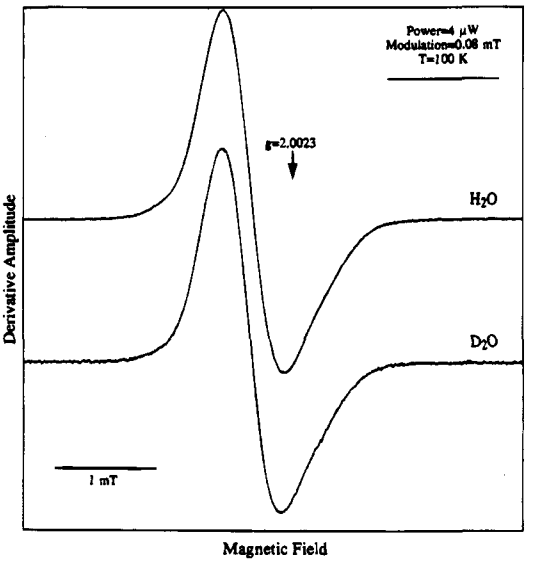

Figure 2. Continuous-wave EPR spectra of randomly oriented *P. denitrificans* methylamine dehydrogenase reduced with dithionite in ^1H_2O and ^2H_2O buffer. *Conditions*: microwave power, 10 μW; microwave frequency, 9.594 GHz; magnetic field modulation, 0.05 mT; modulation frequency, 100 kHz; temperature, 110 K; average of 16 scans.

ESEEM Spectroscopy. A. ^{14}N Hyperfine and Nuclear Quadrupole Interactions. Figure 3 shows ESEEM frequency spectra of dithionite-reduced MADH in ^1H_2O obtained from Fourier transformation of stimulated echo envelopes generated by using the three-pulse, 90°−τ−90°−T−90° microwave pulse sequence. The spectra are dominated by three narrow lines centered at 0.4, 2.1, and 2.5 MHz. These features are assigned to the nuclear quadrupole transition frequencies (ν_Q) of a single ^{14}N (N1) that is near to the condition of "exact cancellation" [38] of the hyperfine and ^{14}N nuclear Zeeman magnetic fields in one electron spin manifold.[39] This assignment is supported by the following: (a) The center frequency of the 2.5 MHz feature equals the sum of the other two ν_Q values. (b) As shown in Figure 4, the positions of these features are insensitive to the external magnetic field strength (B_0) near exact cancellation.[40] (c) The absence of strong features at harmonics of the fundamental ν_Q values in Figures 3 and 4 indicates coupling to a single ^{14}N. The broad feature at 4−6 MHz arises from the $\Delta m_I = \pm 2$, or double quantum (ν_{dq}), energy level splitting in the N1 electron spin manifold where the hyperfine and nuclear Zeeman fields are additive. Comparsion of the positions of the ν_{dq} features in Figures 3 and 4 shows that, as expected, the double quantum feature migrates in proportion to twice the change in the ^{14}N Larmor frequency as B_0 is increased.

Figures 3 and 4 also show features of lower amplitude that arise from interaction of the unpaired spin with a second ^{14}N (N2) for which the hyperfine and nuclear Zeeman fields fail to

(36) Rose, M. E. *Elementary theory of angular momentum*; Wiley and Sons: New York, 1957.

(37) De Beer, R.; Duine, J. A.; Frank, J.; Large, P. J. *Biochim. Biophys. Acta* **1980**, *622*, 370−374.

(38) (a) Mims, W. B.; Peisach, J. *J. Chem. Phys.* **1978**, *69*, 4921−4930. (b) Flanagan, H. L.; Singel, D. J. *J. Chem. Phys.* **1987**, *87*, 5606−5616. (c) Mims, W. B.; Peisach, J. In *Advanced EPR: Applications in Biology and Biochemistry*; Hoff, A. J., Ed.; Elsevier: New York, 1989; pp 1−57.

(39) At exact cancellation a zero-magnetic field condition prevails for one electron spin manifold, that is $A/2 = \nu_N$. For ^{14}N, which has nuclear spin $I = 1$ and therefore an electric quadrupole moment, the zero magnetic field energy levels are the eigenstates of the nuclear quadrupole Hamiltonian, and the energy level splittings are given by the nuclear quadrupole frequencies, ν_Q.[38] The high intensity of the ^{14}N ν_Q features at exact cancellation arises because of the strong mixing of the nuclear eigenstates in the electron spin manifold where the ^{14}N nuclear Zeeman and hyperfine interactions are additive. The state mixing renders comparable the probabilities for classically allowed and forbidden EPR transitions which favors strong ESEEM.[30,31]

(40) Lucken, E. A. C. *Nuclear Quadrupole Coupling Constants*; Academic Press: London, 1969.

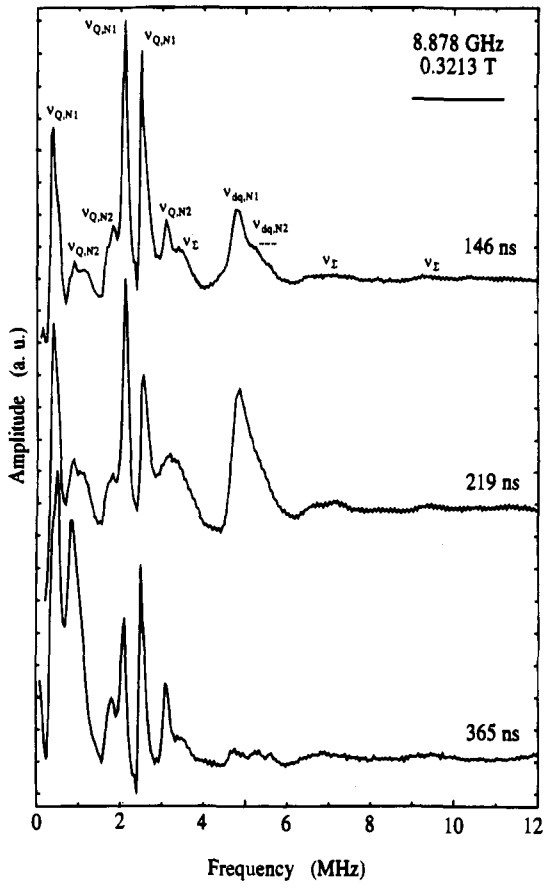

Figure 3. Stimulated-echo ESEEM spectra of the dithionite-generated TTQ-semiquinone in methylamine dehydrogenase. The frequency of the pulsed microwave magnetic field in the ESEEM measurements corresponds to the zero-crossing in the EPR derivative line shape shown in Figure 2. The Fourier transformations of envelope modulation obtained at τ values of 146, 219, and 365 ns are shown. The selected τ values correspond to suppression of the ^{1}H ν_N line. *Conditions*: initial T (T_0), 40 ns; microwave frequency, 8.878 GHz; magnetic field strength, 0.3213 T; microwave pulse power, 40 W (20 ns fWHM); pulse sequence repetition rate, 20 Hz; 10 events averaged per time point; temperature, 4.2 K.

satisfy the cancellation condition. The broadening of these $\nu_{Q,N2}$ features, relative to the $\nu_{Q,N1}$ lines and alterations of their frequency positions with changes in B_0, is caused by the contributions of an orientation-dependent dipolar hyperfine interaction.[38b] Therefore, hyperfine coupling to N2 has a larger anisotropy than to N1. Contributions of N2 to the ν_{dq} feature in the spectra of Figures 3 and 4 are also apparent.

Combination lines can arise in ESEEM spectra when multiple nuclei interact with the same electronic wave function.[38ac,41] Combination lines positioned at multiples of the fundamental and double quantum frequencies of N1 and N2 are displayed in the spectra of Figure 3 and are labeled by ν_Σ. The presence of the combination lines demonstrates that the N1 and N2 nitrogen nuclei are present in the same TTQ radical.

In Figures 3 and 4, differences in the amplitudes and shapes of the features obtained at the different τ values are caused by an interdependence of the amplitudes of the conjugate hyperfine frequencies in the $m_s = +1/2$ (frequency components, $\nu_{\alpha,ij}$, where i and j refer to the nuclear sublevels) and $m_s = -1/2$ ($\nu_{\beta,ij}$) electron spin manifolds that are modulated by τ.[30,31,42] The τ-dependence of the line shape is shown most dramatically

(41) (a) Lin, C. P.; Bowman, M. K.; Norris, J. R. *J. Chem. Phys.* **1986**, *85*, 56−62. (b) McCracken, J.; Pember, S.; Benkovic, S. J.; Villafranca, J. J.; Miller, R. J.; Peisach, J. *J. Am. Chem. Soc.* **1988**, *110*, 1069.

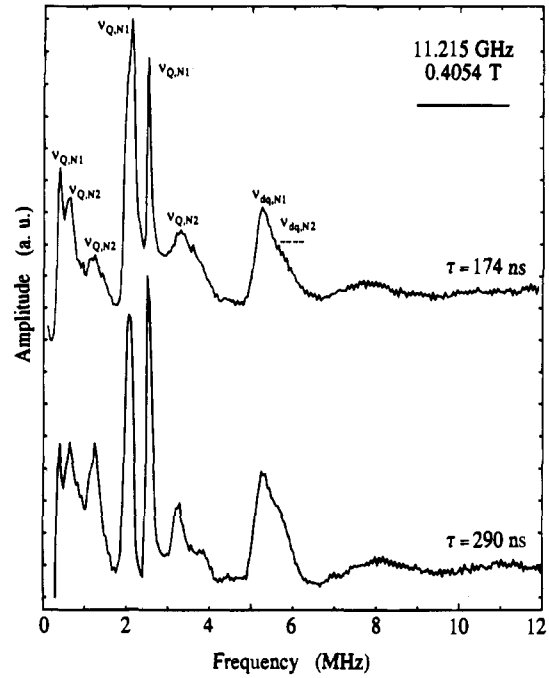

Figure 4. Stimulated-echo ESEEM spectra of the dithionite-generated TTQ-semiquinone in methylamine dehydrogenase. The Fourier transformations of envelope modulation obtained at τ values of 174 and 290 ns are shown. The envelope modulation was collected at higher microwave frequency and magnetic field strength than in Figure 2. *Conditions*: initial T (T_0), 40 ns; microwave frequency, 11.215 GHz; magnetic field strength, 0.4054 T; microwave pulse power, 50 W (20 ns fWHM); pulse sequence repetition rate, 6 Hz; 10 events averaged per time point; temperature, 4.2 K.

in the disappearance of the N1 double quantum feature at higher τ values in Figure 3, and the emergence of the 0.9 MHz N2 feature in Figure 3 with increasing τ. The sensitive dependence of the line shapes on τ value and B_0 provides stringent constraints for ESEEM simulations that are necessary to determine the ^{14}N hyperfine and nuclear quadrupolar coupling tensors.

B. Strong ^{1}H Hyperfine Interactions. Figure 5 shows ESEEM spectra of dithionite-reduced MADH in ^1H_2O and ^2H_2O obtained by using the two-pulse, or Hahn echo, 90°−τ−180° microwave pulse sequence. Lines that arise from the heterodyning of the fundamental ν_α, ν_β conjugate frequencies can be observed in two-pulse ESEEM spectra and are marked by a negative phase.[30,44] The spectral region at >12 MHz is dominated by the ^{1}H Larmor fundamental (ν_N) and narrow sum-combination ($2\nu_N$) lines. The ν_N fundamental arises from weak dipolar hyperfine interaction with the "matrix" ^{1}H nuclei in the protein and solvent media that surround the radical.[26a] In addition, features from combination of the ν_N and $2\nu_N$ lines with

(42) When the value of τ is set equal to an integral number of cycles of one hyperfine frequency component, say $\nu_{\beta,ij}$, the contribution of the conjugate frequency component $\nu_{\alpha,ij}$ to the envelope modulation is suppressed. At half integral values of $(\nu_{\beta,ij})^{-1}$, the envelope modulation at frequency ν_α is relatively enhanced. Suppression effects are complete for $S = 1/2$, $I = 1/2$ systems of axial dipolar hyperfine symmetry.[31] For rhombic symmetry, suppression is partial.[31,43] Suppression effects for ^{14}N coupling near exact cancellation are less systematic than for electron-nuclear interactions where the nuclear quadrupole contribution can be neglected. This is because of the substantial breakdown of the 1:1 correspondence between conjugate ν_α, ν_β frequency values, which is caused by the rhombic symmetry of both the hyperfine field and electric field gradient, and strong nuclear state mixing caused by the quadrupole interaction.

(43) (a) Fauth, J. M.; Schweiger, A.; Braunschweiler, L.; Forrer, J.; Ernst, R. R. *J. Magn. Reson.* **1986**, *66*, 74−86. (b) Fauth, J. M.; Schweiger, A.; Ernst, R. R. *J. Magn. Reson.* **1989**, *81*, 262−274. (c) Warncke, K.; McCracken, J. *J. Chem. Phys.* **1994**, *101*, 1832−1841.

(44) Rowan, L. G.; Hahn, E. L.; Mims, W. B. *Phys. Rev.* **1965**, *137*, A61-A71.

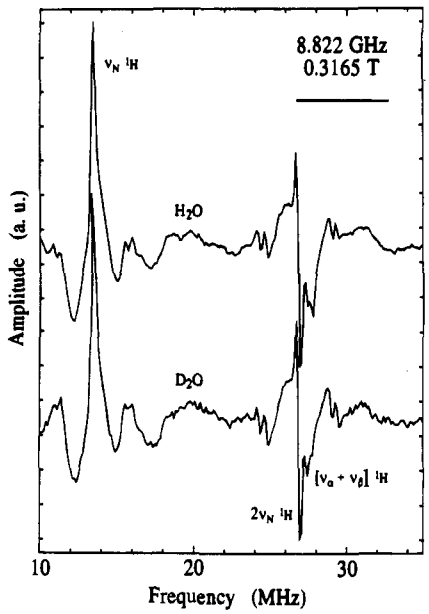

Figure 5. Two-pulse ESEEM spectra of the dithionite-generated TTQ-semiquinone in methylamine dehydrogenase in ^1H_2O and ^2H_2O buffer. *Conditions*: initial τ value, 120 ns; microwave frequency, 8.822 GHz; magnetic field strength, 0.3165 T; microwave pulse power, 40 W (20 ns fWHM); pulse sequence repetition rate, 10 Hz; 10 events averaged per time point; temperature, 4.2 K.

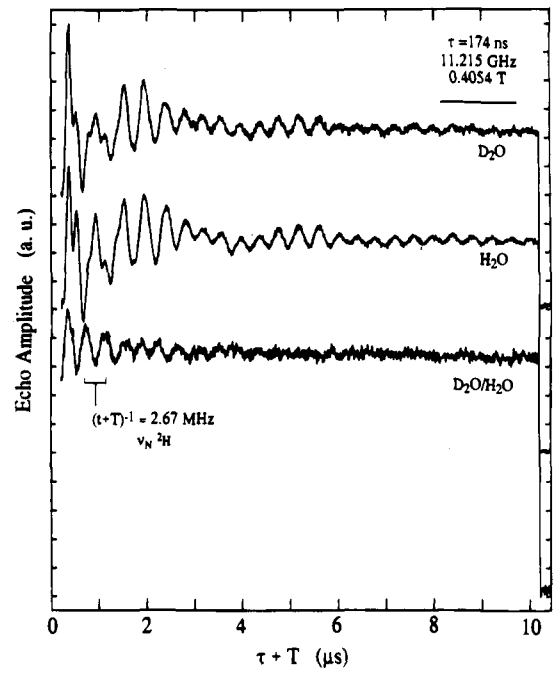

Figure 6. Stimulated-echo envelope modulation from the dithionite-generated TTQ-semiquinone in methylamine dehydrogenase in ^1H_2O and ^2H_2O buffer and quotient modulation. The magnetic field strength was selected to position the ^{2}H Larmor frequency, ν_N, for a minimum of interference from the ^{14}N ν_Q features. *Conditions*: τ, 174 ns; initial T (T_0), 40 ns; microwave frequency, 11.215 GHz; magnetic field strength, 0.4054 T; microwave pulse power, 50 W (20 ns FWHM); pulse sequence repetition rate, 10 Hz; 10 events averaged per time point; temperature, 4.2 K.

the N1 ^{14}N ν_Q lines are observed as splittings and subsplittings displaced symmetrically to each side of the ^{1}H ν_N and $2\nu_N$ lines.[38] Theoretical treatments have shown that $\nu_\alpha + \nu_\beta$ features that are split from $2\nu_N$ arise from strong hyperfine interactions that include a large dipolar component.[45] In the spectrum of the TTQ radical in ^1H_2O buffer, a broad $\nu_\alpha + \nu_\beta$ feature is observed, with minima that are shifted by 0.4 and 0.8 MHz from $2\nu_N$. Therefore, at least two ^{1}H nuclei with a strong dipolar coupling component are present in the TTQ semiquinone. In the spectrum obtained in ^2H_2O, the 0.8 MHz splitting is absent. Thus, the hydrogen nucleus that gives rise to the 0.8 MHz splitting is sensitive to solvent exchange.

C. Hyperfine Interaction with Exchange-Sensitive ^{2}H Matrix Nuclei. The modulation intensity at the ^{2}H Larmor frequency, which is characteristic of the matrix ^{2}H nuclei, provides a qualitative,[46a] or in some cases quantitative,[46b] measure of the accessibility of the unpaired spin density in the TTQ radical to solvent ^2H_2O. Figure 6 shows individual envelope modulation collected for enzyme in ^2H_2O, ^1H_2O, and the quotient envelope. Division of the envelopes eliminates or strongly attenuates modulation components from coupled non-exchangeable nuclei that are common to the radicals in ^1H_2O and ^2H_2O and emphasizes contributions from exchangeable ^{2}H.[38c,44] The quotient envelope in Figure 6 displays a single modulation component with a period of 2.6 MHz that is characteristic of the weak, dipolar hyperfine-coupled matrix ^{2}H. The depth of this modulation is small in comparison with modulation from model radicals in ^2H_2O (Warncke, K.; McCracken, J. Unpublished). Therefore, the unpaired spin density in the TTQ radical is well sequestered from the bulk solvent. The absence of contributions to the ^{2}H ESEEM from strongly coupled, exchangeable ^{2}H nuclei is consistent with the relatively small changes in the EPR line width introduced by solvent exchange.

(45) Reijerse, E. J.; Dikanov, S. A. *J. Chem. Phys.* **1991**, *95*, 836–845.
(46) (a) Mims, W. B.; Davis, J. L.; Peisach, J. *Biophys. J.* **1984**, *45*, 755–766. (b) Mims, W. B.; Davis, J. L.; Peisach, J. *J. Magn. Reson.* **1990**, *86*, 273–292.

CW-ENDOR Spectroscopy. A. Nonsolvent-Exchangeable Hyperfine Interactions. Figure 7 shows proton-ENDOR spectra of dithionite-reduced MADH in ^1H_2O and ^2H_2O buffer over the radiofrequency range of 10–20 MHz that includes the ^{1}H ν_N value of 14.67 MHz. The spectra were obtained under conditions of intermediate spectral resolution[26c] with radiofrequency power of 50 W and modulation depth of 20 kHz. The temperature for optimum amplitude and resolution of all ENDOR transitions was found to be approximately 120 K. Table 1 lists the hyperfine coupling constants with values of >1 MHz, given by the frequency separation between pairs of features that are disposed symmetrically about the ^{1}H Larmor frequency. Hyperfine couplings in the matrix region (<1 MHz) will be addressed in detail in a subsequent work.[24] In the derivative absorption presentation of the ENDOR spectra, the transitions correspond to the extrema of the powder pattern distribution of different hyperfine interactions in the radical. Therefore, the hyperfine couplings represent the principal values of hyperfine tensors of ^{1}H that are coupled to the delocalized, unpaired spin density.

The hyperfine couplings, a-a′, b-b′, d-d′, e-e′, and g-g′ through o-o′, are present in both the ^1H_2O and ^2H_2O spectra and therefore correspond to nonexchangeable ^{1}H hyperfine interactions. Exchangeable ^{1}H hyperfine couplings are identified by their disappearance from the ^{1}H-ENDOR spectrum of the radical prepared in ^2H_2O solvent.[26a] The corresponding deuterium hyperfine transitions would occur near to the ^{2}H Larmor frequency (2.2 MHz) and are thus not observed in the radio-frequency range examined. Identification of the overlapping, nonexchangeable couplings was aided by the selective pronounced asymmetry of the transition intensities at $\nu < \nu_N$ and $\nu > \nu_N$. The transitions, l and o, exhibited enhanced intensity, relative to their high frequency conjugate transitions, whereas the transitions, e′, g′, i′, j′, k′, and n′, were stronger than their

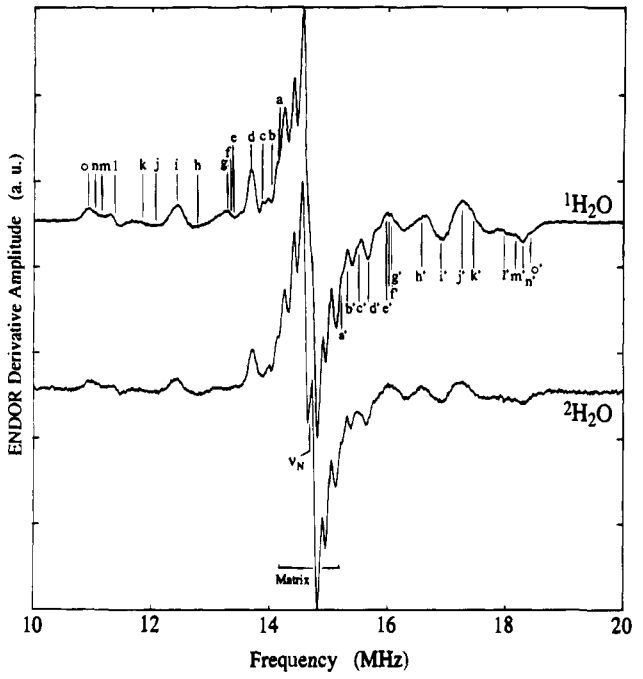

Figure 7. Proton CW-ENDOR spectra of dithionite-generated TTQ-semiquinone in methylamine dehydrogenase in ^1H_2O and ^2H_2O buffer. The ^1H Larmor frequency is 14.67 MHz and corresponds to the zero-crossing of the derivative line shape. The spectra were taken at the maximum EPR absorption, equivalent to the zero-crossing of the EPR line shapes shown in Figure 2. Lower case letters designate pairs of transitions that compose the hyperfine coupling constants that are listed in Table 1. All ENDOR spectra were obtained with the same samples used in the ESEEM studies. *Conditions*: microwave power, 1.6 mW; microwave frequency, 9.654 GHz; $g = 2.004$; rf power, 50 W; FM, 20 kHz; temperature, 148 K. Each spectrum represents the average of 64 (^1H_2O) or 96 (^2H_2O) scans.

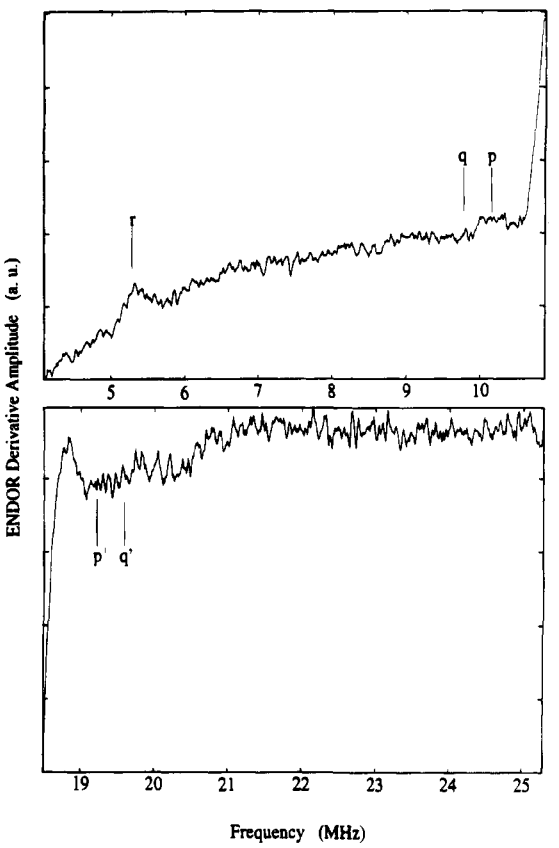

Figure 8. Proton CW-ENDOR spectra of dithionite-generated TTQ-semiquinone in methylamine dehydrogenase in ^1H_2O buffer on the perimeter of the 10−20 MHz radiofrequency range. *Conditions*: microwave power, 1.6 mW; microwave frequency, 9.650 GHz; $g = 2.004$; rf power, 100 W at 5 MHz, 70 W at 10 MHz; 100 W at 20 MHz, 30 W at 25 MHz; FM, 100 kHz; temperature, 140 K. A spectrum obtained under identical conditions but off-EPR resonance by 2 mT has been subtracted to account for baseline disturbances outside of the 10−20 MHz range. Absorption of radiofrequency power carried by odd harmonics of the ^1H Larmor frequency causes the downward slope in the baseline at low frequency.

low-frequency conjugates. The assignments are substantiated by consideration of known hyperfine tensor symmetries, as detailed below.

Figure 8 shows additional transitions of weak intensity for MADH in ^1H_2O buffer that lie outside the ~10−20 MHz range of high-detection sensitivity. These weak transitions are best observed under conditions of high radiofrequency modulation and power, which enhance the signal-to-noise ratio with some sacrifice of spectral resolution.[26c] The hyperfine couplings corresponding to the transitions, p-p′, q-q′, and r, are listed in Table 1. The transition, r′, predicted at 24.1 MHz, is not observed because the radiofrequency power necessary to drive this transition is limited at >22 MHz by mismatch of the line and coil impedances. The features, p-p′, q-q′, and r, were not sensitive to solvent exchange. All of the hyperfine couplings presented in Table 1 are $< \nu_N$, which is consistent with the relatively narrow EPR linewidth.

B. Solvent-Exchangeable Hyperfine Interactions. The hyperfine couplings, c-c′ and f-f′, observed in the ^1H_2O spectrum in Figure 7 are absent in the ^2H_2O spectrum and therefore arise from coupling to solvent exchangeable ^1H nuclei. The ENDOR line shape asymmetry about ν_N is severe for the exchangeable features. The transitions at $\nu > \nu_N$ reproduce faintly the intensity observed at $\nu < \nu_N$.

C. Orientation-Restricted ENDOR. Microwave irradiation at different magnetic field positions in the EPR line allows hyperfine couplings characteristic of a restricted subset of molecular orientations to be addressed in the ENDOR experiment.[26a] Angle-restricted ENDOR spectra are shown in Figure 9. The low spectral resolution in these ENDOR spectra, compared to the spectra in Figure 7, is caused by the high radiofrequency modulation necessary to achieve reasonable signal-to-noise ratios for the low paramagnet concentrations at the perimeter of the EPR spectrum. The line shape differences between the ENDOR spectra obtained at the low and high field extrema of the EPR line show clearly the resonance of a restricted subset of molecular orientations. In particular, the ENDOR spectrum obtained at the high field ($g = 1.999$) position displays distinctly three pairs of hyperfine couplings with the derivative line shapes expected for a restricted band of hyperfine frequencies at 1.6, 2.7, and 6.5 MHz. This is consistent with the lower dispersion in molecular orientations in organic π-radicals at low g-value, relative to high g-value.[47] Two orientation-restricted hyperfine couplings are also observed at 4.1 and 6.3 MHz at high g-value. The relatively large width of the orientation-restricted transitions arises in part from the dispersion in molecular orientations, owing to the low g-anisotropy and high radiofrequency modulation.

The results presented in Figure 9 agree with the ENDOR line shapes obtained in orientation-selection experiments performed at Q-band (33.5 GHz) with lyophilized powder MADH samples.[37] The low g-value spectrum at Q-band exhibits so-called "single crystal-like" derivative line shapes, while the high g-value spectra show less well-resolved hyperfine couplings. In the

(47) Gordy, W. In *Techniques of Chemistry, Volume XV: Theory and Applications of Electron Spin Resonance*; West, W., Ed., Wiley & Sons: New York, 1980.

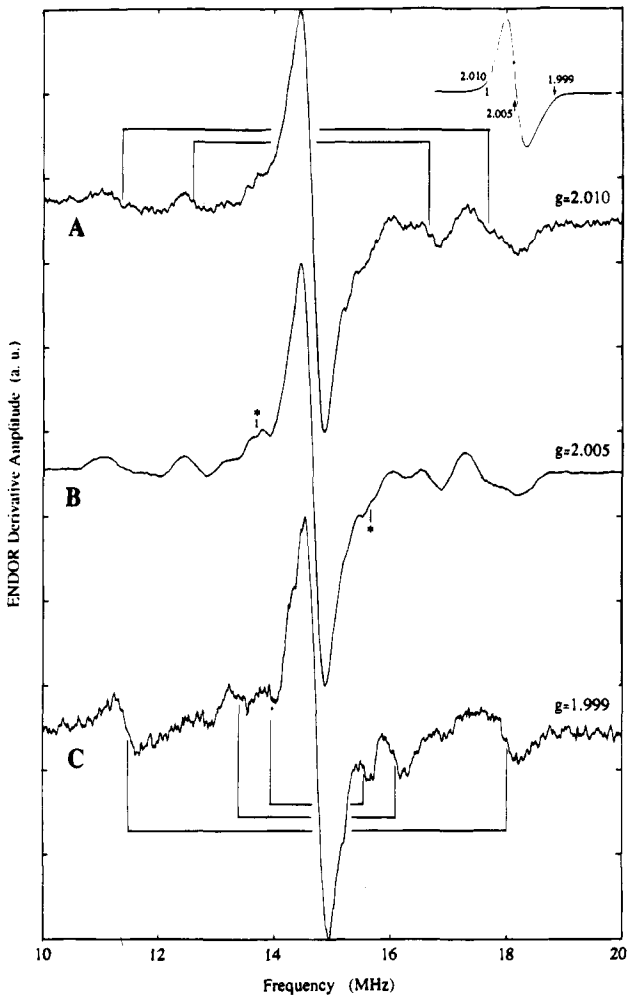

Figure 9. Orientation-restricted ^1H CW-ENDOR spectra of dithionite-generated TTQ-semiquinone in methylamine dehydrogenase in ^1H_2O buffer. The ENDOR spectra correspond to different positions of microwave irradiation in the EPR line shape, as shown in the inset EPR spectrum. (A) Low magnetic field, $g = 2.010$. (B) Center magnetic field, $g = 2.005$. The asterisk shows the frequency position of the feature observed in the low-power, low-modulation ^1H_2O spectrum displayed in Figure 6 at 2.0 MHz. (C) High magnetic field, $g = 1.999$. The spectra are aligned at ν_N, where ν_N is 14.63, 14.67, and 14.72 MHz for A, B, and C, respectively. *Conditions*: microwave power, 1.6 mW; microwave frequency, 9.650 GHz; rf power, 100 W; FM, 150 kHz; temperature, 140 K.

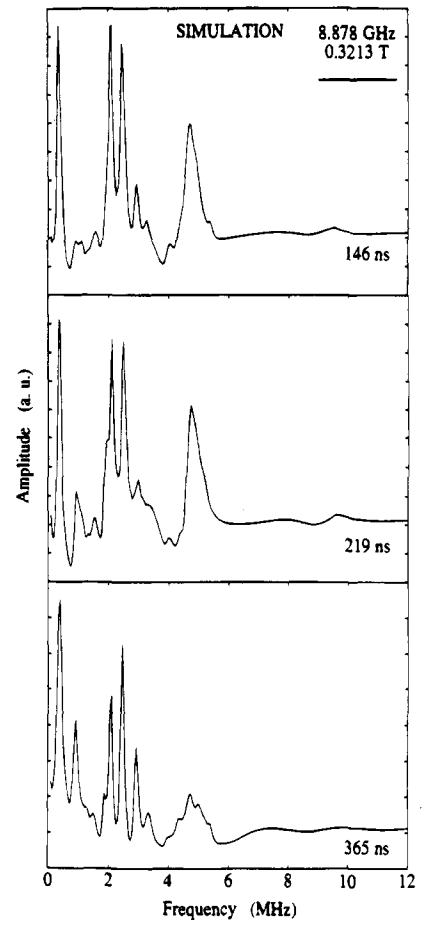

Figure 10. Fourier transformations of theoretical simulations of three-pulse ^{14}N ESEEM from dithionite-generated TTQ-semiquinone in methylamine dehydrogenase. These simulated spectra correspond to the experimental conditions and τ values of 146, 219, and 365 as for the experimental spectra presented in Figures 2. The simulations were performed using two coupled ^{14}N nuclei, N1 and N2, with the hyperfine and nuclear quadrupole parameters listed in Table 2. Modulation from the two ^{14}N nuclei was combined according to the product rule.[30,44] *Simulation parameters*: g_n, 0.4035; magnetic field strength, 0.3213 T; initial value of T, 40 ns. An isotropic electronic g-factor was assumed.

Q-band work, hyperfine couplings of 3.3 and 7.0 MHz were reported at the low g-value (2.0028) that correspond to our values of 2.7 and 6.5 MHz. The comparable line shapes and orientation-restricted hyperfine couplings in the Q- and X-band work indicate that the corresponding hyperfine interactions are affected minimally by dehydration of MADH.

Discussion

^{14}N Hyperfine and Nuclear Quadrupole Interactions. The principal values of the hyperfine tensors and nuclear quadrupole coupling parameters for the two nitrogen atoms, N1 and N2, were obtained from theoretical simulations of the ^{14}N ESEEM spectra. The simulation parameters are listed in Table 2. Figure 10 shows the simulated ESEEM spectra corresponding to the conditions of the experimental spectra displayed in Figure 3. The minor differences between the experimental and simulated spectra are attributed primarily to the assumption of mutual random orientations of N1 and N2 in the simulations and to the assumption of an axial dipolar hyperfine tensor.[48] The combination lines in the ESEEM spectra, which result from the product rule,[30,44] indicate that the signs of the hyperfine coupling for N1 and N2 are the same.

Values of the ^{14}N nuclear quadrupole coupling constant, e^2qQ/h, and, to a less dependable degree, the electric field gradient asymmetry parameter, η, are characteristic of the valence electronic structure of the nitrogen atom.[40,49,50] The values of $e^2qQ/h = 3.0$ MHz and $\eta = 0.2$ obtained for N1 are comparable with the values of 3.01 MHz and 0.18 observed for indole nitrogen in tryptophan powder by pure quadrupole resonance.[50,51] The minor perturbations in the N1 nuclear quadrupole coupling parameters, relative to those for indole nitrogen suggest the assignment of N1 to the N_1 nitrogen atom in the unmodified indole-ring of the TTQ radical. The low η value for the trigonal indole nitrogen arises from the approximately uniform electron populations in the C–N bonds and delocalization of the nitrogen lone pair into the ring.[35] The same η

(48) The essential features of the hyperfine interaction, that is, the strength and the extreme principal values of the hyperfine tensor, are captured in the assumption of the axial dipolar hyperfine field. Efforts are now in progress to converge to the true rhombic tensor values, with the aid of molecular orbital calculations, to quantify hyperfine fields emanating from neighbor nuclei for which experimental spin densities cannot be obtained.

(49) Townes, C. H.; Dailey, B. P. *J. Chem. Phys.* **1949**, *17*, 782.
(50) Edmonds, D. T. *Phys. Lett. C* **1977**, *29*, 233–290.

value for N_1 suggests that the indole ring in TTQ is also planar. The N_1 isotropic coupling could arise from polarization of the ^{14}N valence s-electron density by unpaired p_π spin density resident on N_1 or by a through-bond mechanism from near-neighbor p_π density.[47] The low anisotropy of the hyperfine tensor shows that the through-bond polarization mechanism dominates. This suggests that significant ϱ_π is located on C_2 and $C_{4'}$.

In contrast to N1, the higher e^2qQ/h and η values for N2, although close enough to be consistent with an indole-nitrogen source, indicate an increased strength and higher rhombicity of the electric field gradient about N2. These changes might result from a chemically modified indole ring system, and N2 is therefore assigned to $N_{1'}$ of the indole-quinone sidechain. The slightly higher anisotropy of the $N_{1'}$ dipolar tensor suggests hyperfine coupling is primarily with p_π-electron spin density located on $N_{1'}$. The value of ϱ_π calculated from the isotropic coupling[47] is 0.02. Although the nuclear quadrupole coupling parameters for N2 are similar to those for amide-^{14}N of the terminal amino acid in several tripeptides,[50] it is unlikely that N2 (or N1) is a peptide backbone nitrogen. For example, for unit ϱ_π, the amount of spin density that is observed experimentally to be transmitted through C−C bonds to γ-protons in organic radicals,[52] when scaled appropriately for an sp^2- to sp^3-hybridization of the receiving orbitals and the valence s-orbital coupling of ^{14}N (1540 MHz[33]), yields $|A_{iso}| = 0.50-0.68$ MHz for γ-^{14}N coupling. Calculations based on a model incorporating both polarization and direct mechanisms of spin exchange[53] gives a maximum $|A_{iso}| = 0.98-1.20$ MHz. Thus, to attain the observed A_{iso} values a physically discordant $\varrho_\pi > 1$ is predicted. As described below, ϱ_π at $C_{3'}$ and C_3 is 0.04 and 0.11, respectively.

α-Proton Hyperfine Interactions. Hyperfine couplings given in Table 1 that correspond to the principal values of an α-proton tensor can be identified by comparison with the magnitudes and proportions of the principal values estimated from established physical models.[33,47,54] The dipolar tensor components ($A_{dip,i}$, where $i = x$, y, or z) are calculated by using $R_{CH} = 1.1$ Å, and R_p, the effective distance of the unpaired electron from the carbon center along the p-orbital axis, of 0.7 Å.[47] The isotropic coupling is computed by using the McConnell relation for α-hydrogen coupling,[54] with proportionality constant, Q_α, taken as −69.6 MHz.[27b] Thus, the principal components of the hyperfine tensor, **A**, denoted by $\mathbf{A}_i$, are estimated from the following expression:

$$\mathbf{A}_\alpha{}^{1H} = \varrho_C[A_x,A_y,A_z] = \varrho_C([-4.8, -35.7, 40.1] + [Q_\alpha,Q_\alpha,Q_\alpha]) \text{ (MHz)} \quad (4)$$

The tensor is scaled linearly by the value of the unpaired p_π spin density on carbon, ϱ_C. Simulations of the two-pulse ESEEM spectra displayed in Figure 5 show that the 0.4 MHz splitting of the nonsolvent exchangeable $\nu_\alpha + \nu_\beta$ line from ν_N is consistent with a C−$^1H_\alpha$ interaction with $\varrho_C = 0.16 \pm 0.02$ MHz.

(51) The electric field gradient at the ^{14}N nucleus is created predominantly by the nonbonding, lone-pair electrons.[40,49] Therefore, the small fraction of unpaired electron spin density in the p_π orbital is expected to have a minor influence on the value of the quadrupole coupling constant. Thus, the topa-semiquinone ^{14}N quadrupole coupling can be compared with quadrupole couplings of ^{14}N in crystallographically well-characterized diamagnetic molecules to infer the nuclear and electronic structure.

(52) (a) Fessenden, R. W.; Schuler, R. H. *J. Chem. Phys.* **1963**, *9*, 2147−2195. (b) Eaton, D. R.; Josey, A. D.; Benson, R. E. *J. Am. Chem. Soc.* **1967**, *89*, 4040. (c) Windle, J. J.; Kuhnle, J. A.; Beck, B. H. *J. Chem. Phys.* **1969**, *50*, 2630.

(53) Barfield, M. *J. Phys. Chem.* **1970**, *74*, 621−626.

(54) McConnell, H. M.; Strathdee, *J. Mol. Phys.* **1959**, *2*, 129−138.

Table 1. Proton Hyperfine Coupling Constants and Assignments for the Dithionite-Generated TTQ Radical Determined by CW-ENDOR

transitions	hfc (MHz)	assignment
a, a′	1.1	A_y, $H_{\beta,a'}$
b, b′	1.3	A_x, $H_{\beta,a'}$
c, c′	1.7	na,[b] (exch)
d, d′	2.0	A_z, $H_{\beta,a'}$
e, e′	2.6	A_y, $H_{\beta,b}$
f, f′	2.7	$A_\perp$ O···H (exch)
g, g′	2.8	A_x, $H_{\beta,b}$
h, h′	3.9	A_z, $H_{\alpha,b}$
i, i′	4.5	A_z, $H_{\beta,b}$
j, j′	5.2	A_y, $H_{\beta,a}$
k, k′	5.6	A_x, $H_{\beta,a}$
l, l′	6.6	A_x, $H_{\alpha,b}$
m, m′	6.9	A_z, $H_{\alpha,a}$
n, n′	7.2	A_z, $H_{\beta,a}$
o, o′	7.5	A_x, $H_{\alpha,b}$
p, p′	9.0	A_y, $H_{\alpha,b}$
q, q′	9.7	A_x, $H_{\alpha,a}$
r[c]	18.7	A_y, $H_{\alpha,a}$

[a] Exch, sensitive to ^2H_2O solvent exchange. [b] na, not assigned. [c] Conjugate high frequency transition, r′, is not observed.

In the ENDOR derivative spectra of Figures 7 and 8, the A_y, A_x, and A_z turning points of an α-^1H coupling at $\nu < \nu_N$ would appear with increasing radiofrequency as a positive peak, a derivative feature, and a negative peak, respectively. The order of the transitions and polarity of the excursions is reversed for increasing radiofrequency at $\nu > \nu_N$. The strength and symmetry of the hyperfine couplings q-q′, r, and m-m′ is consistent with a grouping into the A_x, A_y, and A_z components, respectively, of a strongly-coupled α-proton, $^1H_{\alpha,a}$. A ϱ_C value for this α-^1H interaction of 0.17 is computed from the isotropic coupling and eq 4, indicating that this is the same strongly coupled ^1H observed in the ^1H-ESEEM experiments. In this assignment, the parallel amplitude dependence of the l-l′ and o-o′ features on the low (large amplitude) and high (vanishing amplitude) sides of ν_N suggest that these features are part of a single, broad derivative feature. This feature is punctuated with the rise of the $^1H_{\beta,a}$ A_z feature and scalloped by the descending $^1H_{\alpha,a}$ A_z feature, which leads to distortion from the pure derivative line shape. The l-l′ feature is chosen to represent the zero-crossing of the derivative feature. The hyperfine couplings, l-l′, p-p′, and h-h′, can also be accounted for by using eq 4 with $\varrho_C = 0.09$, and therefore are assigned to a second, weaker α-proton interaction, $^1H_{\alpha,b}$. The $^1H_{\alpha,a}$ and $^1H_{\alpha,b}$ principal hyperfine tensor components and estimated ϱ_C values are presented in Table 3.

The structure of TTQ depicted in Figure 1 shows that nonexchangeable α-ring protons are bonded to carbon atoms $C_{2'}$ and $C_{5'}$ of the indole-quinone ring and C_4, C_5, C_6, and C_7 of the indole ring. If the two detected $^1H_\alpha$ interactions were centered at the indole ring positions, the interaction of this substantial spin density with nearby solvent ^2H nuclei would be expected to give ^2H matrix ESEEM more vigorous than observed in Figure 6. We therefore propose that $^1H_{\alpha,a}$ and $^1H_{\alpha,b}$ correspond to the two α-protons bonded to $C_{2'}$ and $C_{5'}$ of the indole-quinone ring of the cofactor.

***β*-Proton Hyperfine Interactions. A. Indole-Quinone Ring System.** The principal values of β-proton hyperfine tensors can be obtained by apportioning hyperfine couplings given in Table 1 according to physical models for the β-interaction.[33,47,55] The principal values of the hyperfine tensor are

(55) Heller, C.; McConnell, H. M. *J. Chem. Phys.* **1960**, *32*, 1535−1539.

estimated by using the following expression:

$$\mathbf{A}_{\beta}^{1H} = \varrho_C[A_x,A_y,A_z] = \varrho_C([-5.1, -7.3, 12.4] + [Q_\beta,Q_\beta,Q_\beta]) \text{ (MHz)} \quad (5)$$

The dipolar components in eq 5 are computed as for eq 4 by using the same R_p value, but with $R_{CH} = 2.1$ Å . In the valence-bond vernacular, the isotropic coupling for the β-interaction is dependent upon the projection of the $C_\beta-H_\beta$ bonding σ-orbitals onto the p_π-orbital axis centered on the ring carbon atom and is related to the dihedral angle, θ, between the $C_\beta-H_\beta$ bond and p-orbital axis according to the following expression:[33,47,55]

$$A_{iso} = \varrho_C Q_\beta = \varrho_C[B_0 + B_2 \cos^2 \theta] \quad (6)$$

For β-methylene ^1H hyperfine coupling in tyrosine radicals oriented discretely by protein, $B_0 \leq (0.004)B_2$ and $B_2 = 167$ MHz,[56] which is comparable with the value of 162 MHz for freely rotating methyl-$^1H_\beta$ in alkyl radicals.[52a] Thus, B_0 is neglected and the isotropic coupling is given by

$$A_{iso} = \varrho B_2 \cos^2 \theta \quad (7)$$

In general, the low anisotropy of the $^1H_\beta$ hyperfine interactions leads to concentration of the ENDOR transitions in a narrower spectral band than for the α-^1H interactions, which leads to enhanced signal intensity.[26a,57]

The ENDOR spectra in Figure 7 show clearly two sets of three nonexchangeable hyperfine couplings, (j-j′, k-k′, n-n′) and (e-e′, g-g′, i-i′), that can be grouped into two low anisotropy β-proton interactions, $^1H_{\beta,a}$ and $^1H_{\beta,b}$, respectively. The common dipolar tensor for these two interactions indicates that they arise from $^1H_\beta$ coupled to the same magnitude of unpaired spin density. This would be expected for coupling of the two methylene-^1H to ϱ_π centered on the ring carbon atom. A value of $\varrho_\pi = 0.11$ is estimated from the dipolar coupling strength. By substituting the two experimental values for A_{iso} into eq 7, and assuming sp^3-hybridization at C_β, values for ϱ_π of 0.11 and θ for $^1H_{\beta,a}$ and $^1H_{\beta,b}$ of 55° and 65° are calculated. The common ϱ_π value calculated from the dipolar and isotropic couplings substantiates the assignments. The $^1H_{\beta,a}$ and $^1H_{\beta,b}$ nuclei are assigned to the indole-quinone methylene bridge linked to $C_{3'}$. The hyperfine coupling parameters and derived spin densities and dihedral angles are presented in Table 3 and the interaction geometry is depicted in Figure 11.

B. Indole Ring System. The assigned interactions, $^1H_{\alpha,a}$, $^1H_{\alpha,b}$, $^1H_{\beta,a}$, and $^1H_{\beta,b}$, exhaust the number of nonexchangeable protons that are bonded to the indole-quinone ring. However, a further set of nonexchangeable transitions of strong intensity and narrow spectral width, corresponding to hyperfine couplings, a-a′, b-b′, and d-d′, are observed in the ENDOR spectra of Figure 7. These hyperfine couplings are sorted into a third β-proton interaction, $^1H_{\beta,a'}$, which is assigned to the methylene bridge of the indole ring.

A θ value for $^1H_{\beta,a'}$ of 62° is obtained from eq 7 with a ϱ_π value of 0.04 estimated from the dipolar tensor and $A_{iso} = 1.5$ MHz. This $\theta_{a'}$ value suggests a model to account for the strong $^1H_{\beta,a'}$ transitions, in which two $^1H_\beta$ with nearly identical θ values of ~60° are coupled to ϱ_π at C_3. The model is supported by the following: (a) the relatively large amplitude of the transitions, which would be promoted by two nearly identical, low anisotropy couplings, (b) the absence of additional strong transitions in the ENDOR spectra corresponding to a second, nonequivalent $^1H_\beta$ interaction, and (c) inflections in the line shape that evidence a slight deviation from equivalence of the two β-^1H couplings. The hyperfine coupling parameters for the two nearly equivalent indole ring β-protons, $^1H_{\beta,a'(b')}$, and the derived spin densities and dihedral angles are presented in Table 3, and the interaction geometry is depicted in Figure 11.

C. Orientation-Selection of β-Proton Interactions. The three strong hyperfine couplings at 1.6, 2.7 and 6.5 MHz that dominate the $g = 1.999$ ENDOR spectrum of Figure 9C represent orientation-restricted ENDOR transitions associated with the $^1H_{\beta,a'(b')}$, $^1H_{\beta,b}$, and $^1H_{\beta,a}$ interactions, respectively, as demonstrated by the following: (a) The hyperfine couplings lie within the nonoverlapping powder pattern line shapes of the $^1H_{\beta,a'(b')}$, $^1H_{\beta,b}$, and $^1H_{\beta,a}$ interactions, that are observed in the

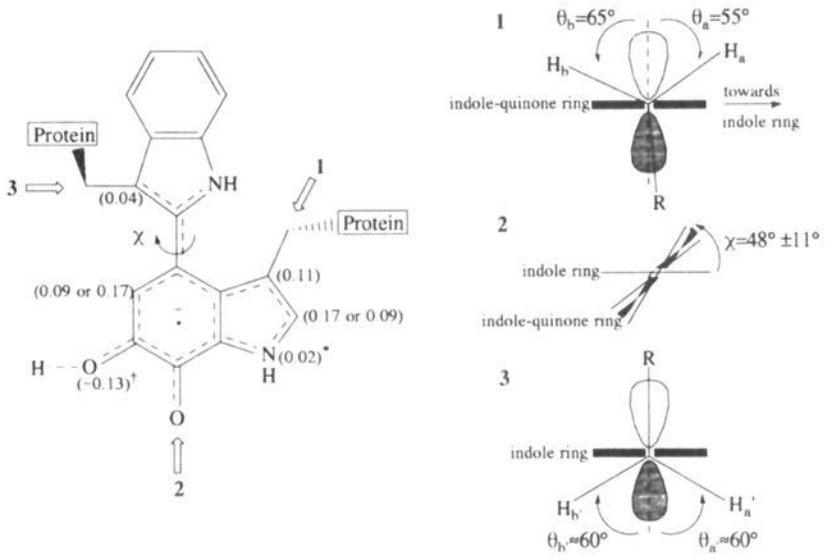

Figure 11. Depiction of the partial unpaired spin density distribution, methylene β-^1H dihedral angles, and inter-ring dihedral angle. The three depictions of the cofactor nuclear geometry at the right are obtained by sighting down the numbered, open arrows (⟹) shown at left. Unpaired spin densities refer to $p\pi$ spin density unless noted otherwise. Dashed lines indicate the detected extent of delocalization of the unpaired spin in the π-system. *Value of p_π ϱ_N required to induce the observed isotropic coupling. A comparable ϱ_N value is also estimated from the dipolar and isotropic parts of the exchangeable hydrogen coupling assigned to N−H. (†Estimated from assumed O···H hydrogen bond distance of 1.5 Å.)

Table 2. Principal Hyperfine Tensor Components, Isotropic and Dipolar Hyperfine Components, and Nuclear Quadrupole Coupling Parameters for ^{14}N Nuclei in the Dithionite-Generated TTQ Radical in MADH[a]

^{14}N nucleus	$\lvert A_\perp \rvert$	$\lvert A_\parallel \rvert$	$\lvert A_{iso} \rvert$	$\lvert A_{dip} \rvert$	e^2qQ/h	η
N1	1.9	2.6	2.1	0.3	3.0	0.2
N2	1.2	2.1	1.5	0.3	3.2	0.6

[a] Hyperfine and nuclear quadrupole coupling values are given in units of MHz.

Table 3. Principal Hyperfine Tensor Components, Isotropic Coupling Constants, Unpaired Spin Densities and β-Proton Dihedral Angles for Proton Hyperfine Interactions in the Dithionite-Generated TTQ Radical in MADH[a,b]

assignment	A_x	A_y	A_z	A_{iso}	$\varrho\pi$	θ
			Nonsolvent Exchangeable			
β-^1H_a	5.6	5.2	7.2	6.0	0.11	55°
β-^1H_b	2.8	2.6	4.5	3.3	0.11	65°
β-$^1H_{a'(b')}$	1.3	1.1	2.0	1.5	0.04	60°
α-^1H_b	−6.6	−9.0	−3.9	−6.5	0.09	
α-^1H_a	−9.7	−18.7	−6.9	−11.8	0.17	
			Solvent Exchangeable			
O···^1H	−2.7	−2.7	(5.4)	(0)	(~0.12)	

[a] Values of the tensor components are given in MHz. [b] In the chosen hyperfine principal axis system, z is along the electron-nuclear vector and x is aligned approximately with the p-orbital axis.

(56) Warncke, K.; Babcock, G. T.; McCracken, J. *J. Am. Chem. Soc.* **1994**, *116*, 7332−7340.
(57) Hyde, J. S.; Rist, G. H.; Eriksson, L. E. G. *J. Phys. Chem.* **1968**, *72*, 4269−4276.

center-field ENDOR spectra shown in Figure 9B as well as in Figure 7. (b) The amplitudes of the transitions are enhanced on the high-frequency side of the ENDOR line, as found for the β-hydrogen hyperfine couplings in the center-field ENDOR spectra of Figures 7 and 9B. The ENDOR line shape asymmetry about ν_N is attributable in part to differences in the rates of cross-relaxation processes between the $m_s = +1/2$ and $m_s = -1/2$ electron spin manifolds.[26a] (c) The relatively large signal amplitudes of the three orientation-restricted hyperfine couplings in the midst of a conflux of transitions from α-^{1}H interactions are consistent with an origin in low anisotropy, β-hyperfine interactions. Since only a single hyperfine coupling falls in the range of values expected for $^1H_{\beta,a'(b')}$, the indole ring β-protons are essentially magnetically equivalent at the molecular orientation corresponding to $g = 1.999$. Comparison of the position of the 2.0 MHz hyperfine coupling in the ENDOR spectra of Figure 7 with the spectra in Figure 9B shows that the inflation of the matrix transition intensity by the higher frequency modulation depth artificially increases the weak hyperfine coupling by 0.14 MHz. Thus, the true $^1H_{\beta,a'(b')}$ hyperfine coupling value at $g = 1.999$ is $1.46 \approx 1.5$ MHz.

Solvent-Exchangeable ^{1}H and ^{2}H Hyperfine Interactions. A. Solvent Interactions. The envelope modulation depth at the ^{2}H Larmor frequency in the quotient envelope of Figure 6 is a measure of the solvent accessibility of the unpaired spin density distributed in the TTQ radical.[46] The modulation depth of 0.16 for dithionite-reduced TTQ in MADH is comparable with the depths we have observed under the same experimental conditions for the cofactor radicals in bovine amine oxidase ($\sim$0.2)[16c] and methanol dehydrogenase (0.22)[58] and is far smaller than modulation depths approaching unity that are observed for model organic radicals in ^2H_2O medium (Warncke, K.; McCracken, J. Unpublished). Therefore, the unpaired spin density on the semiquinone is sequestered from the bulk aqueous solvent and high concentrations of protein interior water. These results suggest that, in the dithionite-generated semiquinone, the majority of the unpaired spin density is localized on the indole-quinone ring of the cofactor which is located in the protein interior.

B. Hydrogen Bonded Interactions. The structure of oxidized TTQ shows that there are four heteroatoms, N_1, $N_{1'}$, $O_{5'}$, and $O_{6'}$, at which solvent-mediated hydrogen exchange could occur. Previous studies have shown that the hyperfine interaction between unpaired spin density on semiquinone or tyrosine radical oxygen atoms and hydrogen-bonded ^{1}H is characterized by a pure dipolar hyperfine interaction,[59] with an attendant traceless, axially-symmetric coupling tensor. The splitting of the solvent-exchangeable $\nu_\alpha + \nu_\beta$ line from ν_N observed in the two-pulse ESEEM spectra of Figure 5 is reproduced in simulations by axially symmetric interaction with $A_{dip} = 2.8 \pm 0.2$ and $A_{iso} = 0$ MHz. This is consistent with the exchange-sensitive derivative-shaped hyperfine coupling of 2.7 MHz, f-f', shown in Figure 7. Associated peak-shaped transitions expected for the largest tensor component, $A_{||}$, of 5.4 MHz are not observed because of the weak intensity for this type of feature when $|A_{||}| > \sim 4$ MHz.[60] The small, unpaired spin densities on N1 and N2 would not be expected to generate an axial N–H coupling feature of this strength. The 2.7 MHz hyperfine coupling is therefore assigned to the perpendicular component, $A_\perp$, of a proton involved in a hydrogen bond to one of the semiquinone oxygen atoms. A crude estimate of the oxygen atom spin density (ϱ_O) of 0.12 is obtained in the point dipole limit by assuming an optimal O···H hydrogen bond distance of 1.5 Å .[61]

C. Covalent Interactions. The hyperfine tensors expected for the interaction of ϱ_π on N2 with the covalently-bonded, exchangeable ^{1}H can be estimated from the ϱ_N value obtained from the ESEEM simulations and values for R_{NH} and R_p of 1.0 Å[62] and 0.7 Å,[47] respectively. The estimated tensor has principal values of |0.6|, |1.5|, and |2.4| MHz (A_{iso} = |1.5| MHz). The exchangeable hyperfine coupling, c-c' (1.7 MHz) may correspond to the intermediate value. High-resolution ENDOR studies are being pursued to identify additional exchangeable N–^{1}H features.

The CW-EPR and ^{2}H ESEEM spectra in Figures 2 and 6, respectively, do not evidence exchangeable hyperfine interactions of the strength expected for a covalent semiquinone O–^{2}H bond. Reported ϱ_O values for semiquinones, obtained from molecular orbital calculations and companion ENDOR studies, are in the range 0.2–0.3.[59a,63] Thus, the results suggest strongly that the two semiquinone oxygen atoms are deprotonated. This is consistent with the low pK_a of semiquinones ($\sim$4–6)[64] and is also supported by the maximum absorption wavelength and extinction coefficient for the UV/visible absorption band of the dithionite-generated semiquinone, which are characteristic of an anionic semiquinone.[22,65] The formal charge on the cofactor radical is therefore −1.

Cofactor Nuclear Geometry. A. Relative Orientation of B_0 and A for $H_{\beta,a}$ and $H_{\beta,b}$ Interactions. The β-^{1}H hyperfine couplings displayed in the orientation-restricted ENDOR spectra correspond to a restricted set of radical orientations relative to $\mathbf{B_0}$. These orientations of $\mathbf{B_0}$, relative to the indole-quinone ring, can be determined from the $H_{\beta,b}$ and $H_{\beta,a}$ hyperfine couplings by following the treatment outlined in Materials and Methods. In order to reduce by two the number of molecular orientations of the TTQ radical necessary to consider, the β-protons are reasonably assumed to be located on the same sides of the rings as observed in the MADH X-ray crystallographic structures.[6,7] Two possible orientations of $\mathbf{B_0}$ remain, corresponding to the cases of $H_{\beta,a}$ ($\theta = 55°$) oriented toward ($H_{\beta,a} = H_{in}$) or away from ($H_{\beta,a} = H_{ex}$) the indole ring. For the $g = 1.999$ data, the surfaces of the $\mathbf{B_0}$ vectors described by the set of [Θ, Φ] values for the hyperfine couplings of 2.7 and 6.5 MHz intersect at values of [$\Theta_b = 83°$, $\Phi_b = 233°$] and at [$\Theta_a = 38°$, $\Phi_a = 233°$] for $H_{\beta,a} = H_{ex}$, and [$\Theta_b = 78°$, $\Phi_b = 71°$] and [$\Theta_a = 40°$, $\Phi_a = 31°$] for $H_{\beta,a} = H_{in}$. For the $g = 2.010$ data, the surfaces of the $\mathbf{B_0}$ vectors described by the set of [Θ, Φ] values for the hyperfine couplings of 4.1 and 6.3 MHz intersect at values of [$\Theta_b = 29°$, $\Phi_b = 0°$] and at [$\Theta_a = 53°$, $\Phi_a = 60°$] for $H_{\beta,a} = H_{ex}$, and [$\Theta_b = 29°$, $\Phi_b = 186°$] and [$\Theta_a = 54°$, $\Phi_a = 230°$] for $H_{\beta,a} = H_{in}$. The unique solutions that are obtained

(58) Warncke, K.; Harris, T. K.; Babcock, G. T.; Davidson, V. L.; McCracken, J. *Biophys. J.* **1994**, *66*, A265.
(59) (a) O'Malley, P. J.; Chandreshekar, T. K.; Babcock, G. T. In *Antennas and Pigments of Photosynthetic Bacteria*; Michel-Beyerle, M. E., Ed.; Springer-Verlag: Berlin, 1985; pp 385–395. (b) O'Malley, P. J.; Babcock, G. T. *J. Am. Chem. Soc.* **1986**, *108*, 3995–4001.
(60) (a) Feher, G.; Isaacson, R. A.; Okamura, M. Y.; Lubitz, W. In *Antennas and Pigments of Photosynthetic Bacteria*; Michel-Beyerle, M. E., Ed.; Springer-Verlag: Berlin, 1985; pp 174–189. (b) Lubitz, W.; Abresch, E. C.; Debus, R. J.; Isaacson, R. A.; Okamura, M. Y.; Feher, G. *Biochim. Biophys. Acta* **1985**, *808*, 464–469. (c) Salerno, J. C.; Osgood, M.; Liu, Y.; Taylor, H.; Scholes, C. P. *Biochemistry* **1990**, *29*, 6987–6993.
(61) Pimentel, G. C.; McClellan, A. L. *The Hydrogen Bond*; W. H. Freeman & Co.: San Francisco, 1960.
(62) Sandorfy, C. In *The Chemistry of the Carbon-Nitrogen Double Bond*; Patai, S., Ed.; Wiley & Sons: London, 1970.
(63) (a) Gendell, J.; Freed, J. H.; Fraenkel, G. K. *J. Chem. Phys.* **1962**, *37*, 2832–2841. (b) Vincow, G. *J. Chem. Phys.* **1963**, *38*, 917–919.
(64) Swallow, A. J. In *Function of Quinones in Energy Conserving Systems*; Trumpower, B. L., Ed.; Academic Press: New York, 1982; pp 59–72.
(65) Morrison, L. E.; Schelhorn, J. E.; Cotton, T. M.; Bering, C. L.; Loach, P. A. In *Function of Quinones in Energy Conserving Systems*; Trumpower, B. L., Ed.; Academic Press: New York, 1982; pp 35–58.

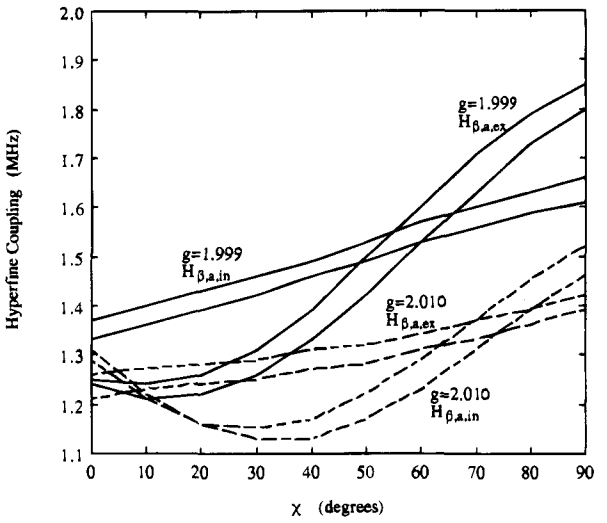

Figure 12. Computed dependence of angle-selected hyperfine couplings for the indole ring β-methylene ^1H nuclei on the inter-ring dihedral angle, χ. The pairs of curves for each g-value and $H_{\beta,a}$ orientation correspond to the hyperfine couplings of $H_{\beta,a'}$ and $H_{\beta,b'}$. The ordinate axis spans the powder distribution of hyperfine transition frequencies determined from ENDOR at the center of the EPR line. In the calculations, the relative orientation of the indole and indole-quinone ring planes is assumed to depend only upon rotation about the $C_2-C_{4'}$ bond, with $\chi = 0°$ defined for coplanar rings, and $\theta = 60°$ for both $H_{\beta,a'}$ and $H_{\beta,b'}$ is assumed.

are not a necessary result of the formalism and therefore demonstrate the consistency and hence substantiate the validity, of the $H_{\beta,a}$ and $H_{\beta,b}$ tensors determined from the powder ENDOR measurements, the measured orientation-restricted ENDOR hyperfine coupling values, the assumed molecular geometry of the TTQ cofactor, and the assumed mutual orientation of the hyperfine and molecular tensor axes.

The two possible $\mathbf{B_0}$ orientations for $g = 1.999$ diverge significantly from colinearity of $\mathbf{B_0}$ with the ring plane normal vector. Since the low g-value in organic π-radicals is achieved when $\mathbf{B_0}$ is aligned along the p-orbital axes parallel to the ring plane normal,[47] our X-band ENDOR results and their consistency with the Q-band angle-selection ENDOR on MADH[37] demonstrate that the angle selection arises primarily from hyperfine anisotropy.

B. Mutual Orientation of the Indole and Indole-Quinone Rings. Figure 12 shows the hyperfine coupling of $H_{\beta,a'}$ and $H_{\beta,b'}$ as a function of χ that are computed from substitution of the two $\mathbf{B_0}$ orientations determined from the $H_{\beta,b}$ and $H_{\beta,a}$ orientations into eq 3. In Figure 12, the $\mathbf{B_0}$ is fixed relative to the indole-quinone ring, but its orientation with respect to the indole ring changes with rotation about $C_2-C_{4'}$ by χ. The $g = 1.999$ data are chosen for estimation of χ because of the enhanced molecular orientation restriction. Figure 12 shows that the $\mathbf{B_0}$ orientation generates an approximately equivalent hyperfine coupling for $H_{\beta,a'}$ and $H_{\beta,b'}$ for all χ. This is consistent with observation of a single hyperfine coupling for $H_{\beta,a'}$ and $H_{\beta,b'}$ at $g = 1.999$. The computed average value for the $H_{\beta,a'}$ and $H_{\beta,b'}$ hyperfine couplings matches the value of 1.5 MHz derived experimentally for the two possible orientations of $H_{\beta,a}$ at 48° ± 11° ($H_{\beta,a} = H_{in}$) or 54° ± 4° ($H_{\beta,a} = H_{ex}$). The uncertainties in χ are calculated from Figure 12 by assuming a rough limit on accurate determination of the hyperfine couplings of ±0.05 MHz. The distinct hyperfine coupling predicted for $H_{\beta,a'}$ and $H_{\beta,b'}$ at $g = 2.010$ by the computations is not observed experimentally. Although the increased bandwidths of the $H_{\beta,a}$ and $H_{\beta,b}$ hyperfine couplings at $g = 2.010$ suggest that this is in part caused by a greater dispersion in molecular orientations at the axial side EPR spectrum, the failure to observe any strong turning-point transition intensity suggests that the $H_{\beta,a'(b')}$ hyperfine coupling may lie at the low-frequency extremum of the powder transitions. In this case, the transitions are likely to be rendered indistinct by the overlapping matrix region transitions, especially at the high modulation depth used in the experiments. The $g = 2.010$ curve for the condition, $H_{\beta,a} = H_{in}$, in Figure 12 shows the smallest hyperfine couplings over the range of χ where the observed and calculated hyperfine couplings at $g = 1.999$ intersect. Thus, we propose that $H_{\beta,a} = H_{in}$ is the correct orientation and, therefore, that $\chi = 48° \pm 11°$.

Comparison of Nuclear Geometries in the Oxidized and Semiquinone States of TTQ in MADH. The indole and indole-quinone methylene group conformations in the oxidized state of TTQ in crystals of MADH indicate that the dihedral angles of each β-hydrogen is 60° ± 5°.[6,7] Comparison of these θ values with our results therefore shows that there is a negligible degree of rotational reorientation about the $C_{3'}-C_{\beta'}$ and C_3-C_β bonds upon direct reduction of oxidized TTQ to the semiquinone. This suggests that the protein around the cofactor has also not changed conformation significantly. The θ values of approximately 60° correspond to the equilibrium position of the broad, double-well torsion potential profile for internal rotation about $C_{ring}-C_\beta$.[66,67] This suggests that there is negligible internal strain, and hence no stored potential energy, in the $C_{3'}-C_{\beta'}$ and C_3-C_β bonds in the methylene bridges to the polypeptide backbone in the oxidized and semiquinone states. Relaxed β-methylene conformations are common among other amino acid-derived cofactor radicals examined thus far,[56,68] with the exception of the tyrosyl radical in ribonucleotide diphosphate reductase.[27b,69]

The value of χ determined by X-ray crystallography for the oxidized state of TTQ in MADH from *P. denitrificans* is 42°.[6,7] A value of 44° was found for the enzyme from *T. versutus*.[8] Both of these values are comparable with our value estimated for the TTQ semiquinone. Stasis of χ with reduction is fully consistent with the absence of significant reorientation of the β-methylene group. Therefore, single electron reduction of the oxidized TTQ cofactor does not cause significant rotation of the two indole ring systems about the $C_2-C_{4'}$ bond.

Implications for the Mechanism of Oxidation of Reduced MADH. A. Dependence of Cofactor-Protein Nuclear Geometry on Enzyme Redox State. The comparable nuclear geometry of the oxidized and semiquinone TTQ cofactor in MADH indicates that redox-elicited changes in protein-cofactor solvation free energy, which would be associated primarily with the generation of negative charge on the cofactor upon semiquinone formation,[70] do not trigger significant, stable cofactor or protein conformational changes. Any gain in resonance stabilization energy from reorienting the indole and indole-quinone rings for optimum π-electron delocalization is also not sufficient to drive conformational changes. This is consistent with the expectation from simple resonance theory[71] that the fully $\pi-\pi$ coupled semiquinone would be antiaromatic (20

(66) Sealy, R. C.; Harman, L.; West, P. R.; Mason, R. P. *J. Am. Chem. Soc.* **1985**, *107*, 3401−3406.
(67) Warncke, K.; McCracken, J. *J. Chem. Phys.* **1995** (in press).
(68) (a) Hoganson, C. W.; Babcock, G. T. *Biochemistry* **1992**, *31*, 11874−11880. (b) Essenmacher, C.; Kim, S. T.; Atamian, M.; Babcock, G. T.; Sancar, A. *J. Am. Chem. Soc.* **1993**, *115*, 1602. (c) Rigby, S. E. J.; Nugent, J. H. A.; O'Malley, P. J. *Biochemistry* **1994**, *33*, 1734−1742. (d) Shi, W.; Hoganson, C. W.; Espe, M.; Bender, C. J.; Tsai, A.-H.; Babcock, G. T. Manuscript in preparation.
(69) Sahlin, M.; Graslund, A.; Ehrenberg, A.; Sjoberg, B.-M. *J. Biol. Chem.* **1982**, *257*, 366.
(70) Warncke, K.; Dutton, P. L. *Biochemistry* **1993**, *32*, 4769−4779.
(71) Coulson, C. A. *Valence*; Oxford University Press: New York, 1961.

π-electrons, including the two nitrogen lone pairs), although resonance effects would be muted by the large delocalization extent.

The results obtained here for the TTQ radical in isolated MADH suggest that changes in χ do not contribute significantly to the mechanism of oxidation of the hydroquinone to quinone.[72] However, the structure of the TTQ semiquinone in isolated MADH does not address the possibility of a different responsivity of protein and cofactor conformation to redox changes when complexed with amicyanin.

B. Inter-Ring Partitioning of the Unpaired Spin Density. The delocalization of the singly-occupied molecular orbital (SOMO) containing the "transferrable electron" [74] is revealed by the unpaired spin density distribution in the TTQ radical. We have mapped this distribution partially. The dominant portion of ϱ_π observed directly (87%) is localized on the indole-quinone ring system. However, the β-hyperfine coupling of the indole ring methylene protons and the hyperfine coupling of the indole ring nitrogen demonstrate that unpaired spin density is delocalized to the indole ring. Partitioning of ϱ_π into the indole ring system is thus not thwarted completely by the observed twisting about the $C_2-C_{4'}$ bond. The delocalization of the SOMO onto the indole pyrrolyl ring is consistent with the intramolecular $\pi-\pi$ coupling predicted from the mutual projections of the component p-orbital axes, which exhibit a cosine-squared dependence.[71] The degree of $\pi-\pi$ overlap for $\chi = 48° \pm 11°$ is predicted from this simple model to be 0.45 (uncertainty limits: 37°, 0.64; 59°, 0.27). The low ^2H_2O solvent accessibility of the unpaired spin density and the absence of ^1H hyperfine couplings of significant strength in the ENDOR spectra in addition to those assigned to the indole-quinone and fused pyrrole ring of the indole ring systems suggest that there is no further significant extension of the SOMO to the annelated benzenoid ring of the unmodified indole.

The delocalization of ϱ_π onto the indole ring system of the semiquinone is consistent with electron departure from the indole ring, as proposed on the basis of the interpretation[17,18] of kinetic[7,19] and X-ray structural[7,19] results in terms of theoretical treatments of electron transmission through protein.[20,21] However, the observed ϱ_π distribution extent suggests electron transfer distances that are approximately 2–4 Å greater than those estimated.[17,18]

The observed partitioning of ϱ_π into the indole ring system provides insight into factors that may be important in the oxidation mechanism of the aminohydroquinone and aminosemiquinone in the native MADH oxidation sequence. The partitioning shows that, in the native reactions, active site chemical transformations can have a direct influence on the unpaired spin density distribution in the absence of large-scale conformational changes. Thus, the overlap of the electronic wave function of the cofactor with the wave functions of protein-external oxidants can be controlled directly by chemical events at the active site.

Acknowledgment. This work has been supported by NIH grants GM-41574 (V.L.D.) and GM-45795 (J.M.) and GM-37300 (G.T.B.).

JA950305R

(72) Since the quinone and semiquinone states have comparable free energies (difference in electrochemical potential, ~0.03 V)[18] and are both deprotonated, the Hammond postulate of structural complementarity between states of comparable energy suggests that there is no significant rotation about χ in the intervening transition state.[73] The Hammond postulate may be invoked to suggest that there is also no significant rotation about χ in the transition state between hydroquinone and quinone, though with less certainty, because the magnitude of the free energy difference is larger (~0.19 V),[17,18] and this step is associated with a double deprotonation of the cofactor.

(73) Hammond, G. S. *J. Am. Chem. Soc.* **1955**, *77*, 334.

(74) Newton, M. D. *Chem. Rev.* **1991**, *91*, 767–792.